DOI: 10.21062/mft.2025.057 © 2025 Manufacturing Technology. All rights reserved. http://www.journalmt.com

Surface Morphology and Ablation Efficiency in UV Ultrafast Laser Micromachining of Fused Silica

Jan Novotný (0000-0001-6175-869X)^{1,2}, Libor Mrňa (0000-0002-3928-5619)², Josef Sedlák (0000-0002-9819-8259)¹, Štěpán Kolomý (0000-0003-3781-692X)¹

¹Institute of Manufacturing Technology, FME, Brno University of Technology; Technická 2896/2, 61669 Brno, Czech Republic. E-mail: Jan.Novotny17@vut.cz

Fused silica is a key material for high-precision applications such as micro-optics and microfluidics. One route to improving direct laser writing (DLW) of fused silica is the use of shorter laser wavelengths, which enable tighter focusing and enhanced absorption. In this study, the influence of process parameters on surface quality and material removal during DLW using a deep ultraviolet (DUV) ultrafast laser (257 nm, 1 ps) was investigated. A full-factorial design of the experiment was used to identify conditions that optimise both surface quality and ablation efficiency. Surface roughness as low as $S_a \approx 200$ nm and material removal rates up to 0.048 mm³·min⁻¹ were achieved. Conditions that led to surface degradation were also identified. Finally, the optimised parameters were applied to fabricate a microfluidic demonstrator. These results confirm that DUV ultrafast DLW is a powerful technique for fabricating high-fidelity features in fused silica with exceptional precision and quality that can be used for micro-optics or microfluidics devices.

Keywords: Ultrafast, Laser, Fused Silica, Micro-processing, Microfluidic

1 Introduction

Fused silica is a widely used material in microfluidics and optics due to its high thermal stability, chemical inertness, toughness and excellent optical transparency [1, 2]. However, its toughness and brittleness pose significant challenges for mechanical methods of (micro) processing; the machining usually causes fracturing of the material, and the tools are a limiting factor for the minimal size of the features [3].

Traditionally, intricate shapes in the brittle materials are made by various etching techniques [4, 5]. Although significant work has been done, several steps are usually needed, including masking and etching in various hazardous chemicals. Etching can also be used in conjunction with lasers in some processes, like FLICE, where a slight modification in the structure greatly enhances the material etching rate [6]. Another example of a method for laser-based manufacturing of glass is laser-induced plasma etching (LIPE), based on the creation of reactive ions in gases near the desired location [7].

The direct laser writing (DLW) technique is a proven technology enabling precision structuring, hole drilling and creation of precision surfaces in a wide range of materials [8–10]. For ultrafast lasers, the first harmonic wavelength, just above 1 µm, is most commonly used. To enhance absorption in transparent dielectrics and reduce the focal spot, second

(515 nm – 532 nm) or third (around 350 nm) harmonic wavelengths are currently used [11–13].

Due to advances in laser output power and harmonics generation efficiency, stable fourth and even fifth-harmonic wavelength lasers (both thin-disk and fibre) are available, and their parameters highly exceed microprocessing needs [14–16]. Although DUV wavelength offers benefits of very low residual heat affected zone, higher absorption, tighter focal spots, and lower threshold fluences, they are used sparsely due to available optics limitations, more demanding beam handling, and safety concerns [17, 18].

Despite the benefits, only limited use of ultrafast DUV lasers for the fabrication of transparent materials has been reported. Häfner reported highly efficient absorption of a 257 nm laser during the cutting of polymer foils, which required only half the power of a 515 nm wavelength [19]. Cho minimised damage and post-processing in the cutting of thin glass by exploiting the DUV ultrafast laser [20]. Stonyte demonstrated ablation with a 206 nm femtosecond laser in a single-spot machining configuration [21].

Although ultrafast DUV lasers offer advantages for processing transparent materials, their application to fused silica has mainly been limited to static or single-spot studies. In this work, we investigate the influence of laser fluence, scan speed, and hatching distance on surface roughness and material removal using a galvo scanner with an F-theta telecentric lens

²Institute of Scientific Instruments, Czech Academy of Sciences, Královopolská 147, 612 64 Brno, Czech Republic.

and a fourth-harmonic ultrafast laser (257 nm, up to 4 W, 60 kHz). We demonstrated that galvo-based DUV processing enables the fabrication of complex microfluidic structures in fused silica with good quality and reasonable throughput.

2 Experimental

Rectangular polished fused silica (15 mm × 28 mm, 2 mm thickness) samples were processed using a microprocessing station based on the Perla 100 (Hi-LASE, Dolní Břežany, CZ) thin-disk regenerative amplifier laser system. The system operates at a fundamental wavelength of 1030 nm. It can output pulses < 2 ps with a maximal energy of 1 mJ at a pulse repetition frequency of 60 kHz (maximal average power of 60 W) with a Gaussian spatial mode (M² < 1.3) and linear polarisation. The fundamental wavelength can be converted to the second (SHG) harmonic (515 nm) with a maximal energy of about 0.4 mJ, and fourth (FHG) harmonic wavelength (257 nm). Maximal energy at 257 nm is measured at 0.068 mJ (4.1 W), and the beam quality parameter M2 is typically lower than 2.2 at the end of beam delivery.

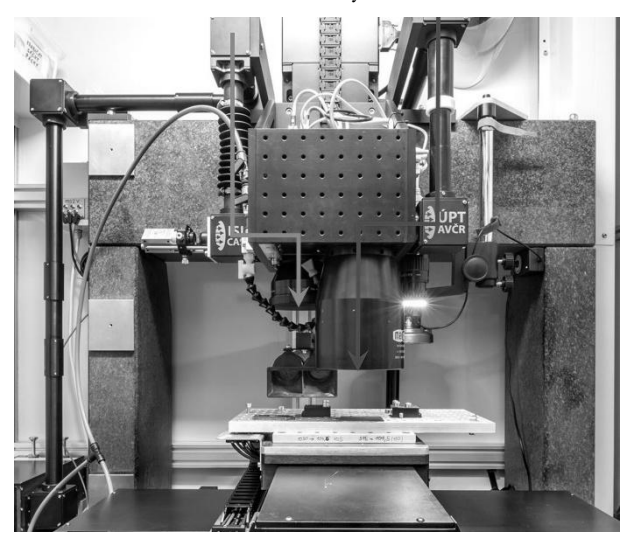


Fig. 1 Processing station, violet line indicates beam delivery path for 257nm, green indicates path for 1030 nm and 515

For this experiment, the beam was routed, as shown in Fig. 1, through an intelliSCAN 14 (Scanlab, Puchheim, DE) scan head to a 100 mm focal length telecentric F-theta lens (Meopta, Přerov, CZ). This setup yielded a focal spot of a diameter of about 7 µm over the scanning field of 15 mm × 15 mm. The samples were positioned on an industrial XY table, and the focus was controlled by a precise Z-stage (MKS Instruments, Andover, MA). The entire process was controlled through DMC laser processing software (Direct Machining Control, Vilnius, LT).

2.1 Samples processing

First, the samples of fused silica for the evaluation of laser fluence and ablation efficiency were machined. For all the following tests, a cross-hatching (0°/90°) laser scanning strategy was chosen to reduce the effects of galvo scanner irregularities [22]. To calculate the pulse energy and laser fluence (according to Eq. 1), the average laser power was measured using thermal power meter S425C (Thorlabs, Newton, NJ) before processing each area. Two sets of regions of dimension $0.4 \text{ mm} \times 0.4 \text{ mm}$, one on the polished surface and one on the pre-machined areas, were made. $F = \frac{2 \cdot Ep}{\pi \cdot d^2} [J \cdot cm^{-2}], \qquad (1)$

$$F = \frac{2 \cdot Ep}{\pi \cdot d^2} \left[J \cdot cm^{-2} \right],\tag{1}$$

Where:

E_p...Pulse energy []],

d...Beam diameter [cm].

Scanning parameters for this experiment were selectected in the middle of possible values, that result in overlapping pulses – scan speed of 200 mm·s⁻¹ and hatching line distance of 3.606 µm, which both resulted in roughly 50 % overlap, pulse overlap (PO, see Eq. 2) in the direction of scan speed and line overlap (LO, see Eq. 3) in the direction of hatching distance were calculated according to [23]. The ablation was repeated 20 times on each area to enhance the accuracy of the measurement. The laser fluence $F = 8.5 \text{ J}\cdot\text{cm}^{-2}$ for pre-machining areas was chosen to be at least 2-3 times the possible F_{th} [17], considering a probable increase due to longer pulses to ensure homogeneous ablation. Table 1 summarises power settings for each

$$PO = \left(1 - \frac{v_s}{d*f_{rep}}\right) \cdot 100 \% [-],$$
 (2)

v_s...Scan speed [mm.s⁻¹],

d...Beam diameter [mm],

f_{rep...}Laser pulse repetition frequency [Hz].
$$LO = \left(1 - \frac{HD}{d}\right) \cdot 100 \%, \tag{3}$$

Where:

HD...Hatching line distance [mm],

d...Beam diameter [mm].

Tab. 1 Laser parameters for F_{th} testing. Att – Attenuator rotation angle, P_{av} – average power, E_p – pulse energy, F – peak fluence

Att [°]	11.5	12.5	13.5	14.5	15.5	16.5	17.5	18.5	19.5	20.5	21.5	22.5	23.5	24.5	25.5
P _{av} [mW]	30	36	42	49	55	62	69	77	84	92	99	107	115	122	130
E _p [μJ]	0.50	0.60	0.70	0.81	0.92	1.04	1.16	1.28	1.40	1.53	1.66	1.79	1.91	2.04	2.17
F [J·cm-2]	2.61	3.12	3.65	4.21	4.79	5.39	6.01	6.65	7.30	7.96	8.62	9.28	9.95	10.61	11.26

Keyence VK-X 1000 (Keyence, Osaka, JP) laser scanning confocal microscope was used to evaluate the depth of machined areas. The depth was measured as the average depth from an area of $0.3 \text{ mm} \times 0.3 \text{ mm}$ square centred in the analysed cavity.

The full factorial design of the experiment was used to evaluate the influences of laser fluence, scan speed, and hatching distance. Due to the galvo scanner's limited resolution, only specific values of hatching distance were suitable for processing. Other

values result in distinct moire-like (grid of hatching and "grid" of a scanner's possible positions) pattern formation as a result of offsetting of the scanned line. The range of scan speeds was selected to have a similar overlap (PO) as hatching (LO). Laser fluence was limited by low LIDT values of available optics for beam routing; nevertheless, the range covers a region of $F/F_{th} < 4$, where optimal efficiency and little to no cracking can be expected [24].

	Tab. 2 Factor values	for evaluation	of process	parameter influence	(HD – hatchi	ng distance, v	- scan streed
--	-----------------------------	----------------	------------	---------------------	--------------	----------------	---------------

Factor			Values									
HD [µm]	1.050 1.585		2.140 2.57		5	3.050	3.606		4.080	4.675	5.105	
LO [%]	85 77		69	63		56	48		42	33	27	
v _s [mm.s ⁻¹]	60		120		180		240			300		
PO [%]	86		71		57		43			29		
F [J.cm ⁻²]	3.8		5.7		7.6		9.5			11.4		
P _{av} [mW]	44		66			88		110			132	
F/F _{th} [-]	1.23		1.84		2.45			3.06		3.68		

The test areas of 0.6 mm \times 0.6 mm were premachined to a depth of (1.36 \pm 0.10) μ m with the same parameters as in the threshold fluence experiment, and the surface was cleaned of debris with filtered compressed air prior to parameter variation. The number of repetitions of scans on each area was chosen to yield \sim 106 pulses. As a result of specifying parameters that were known to result in a surface without pronounced texture, the actual number of pulses per area varied between $8.39 \cdot 10^5$ and $1.36 \cdot 10^6$ with an average of $1.03 \cdot 10^6$ pulses per area.

Areas were grouped by the applied laser power, which was measured before each setting. After machining, the sample was cleaned in an ultrasonic cleaner to remove dust. The measurement was carried out using the VK-X 1000 microscope. The depth of the cavities was measured as the average depth of the central 0.5 mm × 0.5 mm area with respect to the original surface. The depth of premachining was subtracted, and values were normalised to an equivalent dose of

1.106 pulses.

The surface roughness S_a was measured with an L-filter (high pass) of 0.05 mm to retain only a portion of the overall waviness according to EN ISO 25178 [25]. Since the ISO standard recommended a value of S-filter (low pass) of 0.8 μ m, which was lower than the applicable settings, no value was used. No F-operation (surface-shape correction) was applied.

3 Results and discussion

First, the laser threshold fluence of polished and pre-roughened fused silica and corresponding ablation efficiency were evaluated based on the measured depths of cavities shown in Fig. 2. No visible colour changes of the material, which could indicate sub-ablation threshold damage, were observed. The areas with no solid ablation (pre-roughened 11.5 & 12.5 and polished up to 14.5) were omitted from further analysis.

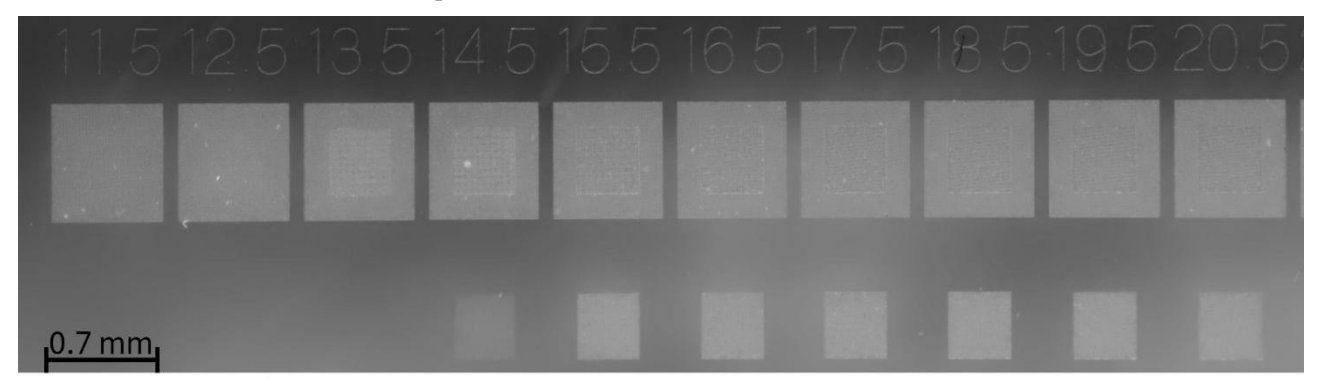


Fig. 2 Sample areas for the F_{th} evaluation, top row with pre-roughened surface, bottom for polished [partial image]

Fig. 3 shows the depths of the cavities per 20 linear hatching passes in the semi-log coordinates. Based on the linear fit, the F_{th} of the polished surface was determined at the value of 4.95 J·cm⁻², whereas with premaching, the threshold fluence lowered to 3.11 J·cm⁻² for 50 % pulse overlap. This lowering is vital for high-precision ablation, where pre-machining ensures repeatable layer-to-layer material removal.

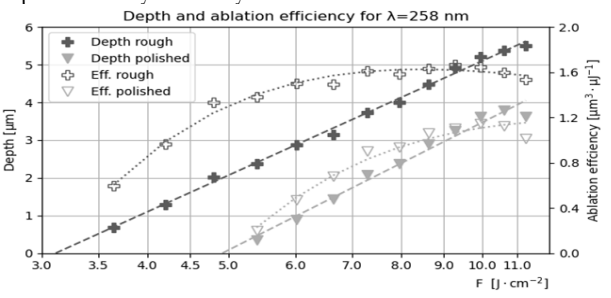


Fig. 3 Ablation depth (semi-log fit dashed) and ablation efficiency

A Peak in the ablation efficiency, which has been reported at an F/F_{th} value of approximately 3 [26], was not observed for the polished surface due to the selected range of fluence. For the pre-roughened surface,

the highest efficiency was calculated at 9.5 J·cm⁻², which corresponded to the aforementioned accepted value for near-single pulse ablation. All used parameters led to only a low-fluence gentle ablation regime, as the data showed no sudden increase in the depth of the cavity.

3.1 Surface texture

Although most of the test areas showed no cracking, edge chipping or discolouration, some defects were observed; examples of these are shown in Fig. 4. The first type (Fig. 4a) was the most common. It consisted of distinct periodic lines protruding about 1.5 µm above the main surface. The period and angle depended on the exact hatching distance settings, as they were caused by an "interference" as discussed in the Experimental section. These had only a minor impact on the roughness value, as they were sparse and of low height.

In some cases (HD of 4.08 μ m and 4.675 μ m), this effect was further enhanced, resulting in up to 10 μ m deep surface structures (Fig. 4b) with a period in the range of hundreds of μ m. These were caused by a speed discontinuity, adding to the directional discontinuity.

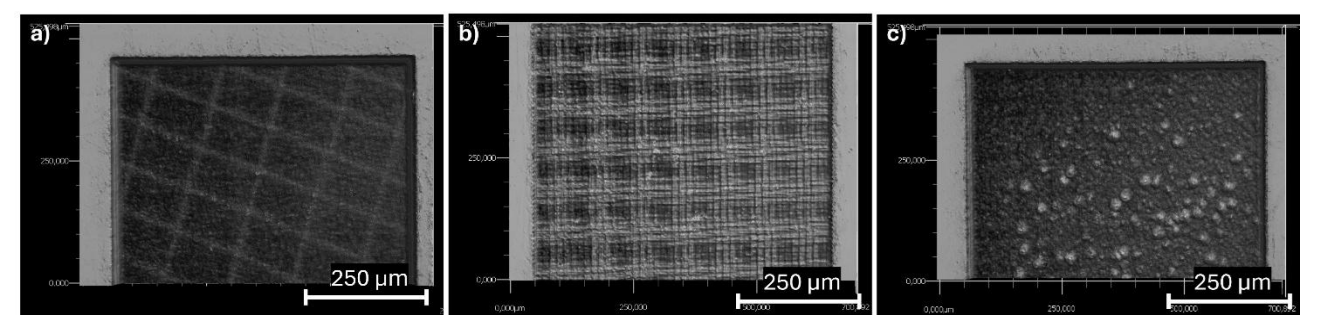


Fig. 4 Main types of surface defects: a) periodic lines, b) pronounced deep long-period structures, c) remelted debris

The second main observed type of defects is shown in Fig. 4c. These random protrusions/bumps were detected exclusively at the highest fluence and lowest scanning speed, which suggests they were caused by high parasitic heating. They were attributed to the redeposition and remelting of ablated particles.

The values of an average surface roughness, Sa, were obtained and are shown in Figure 5 for each fluence. The lowest value is highlighted by a red contour. In general, the average surface roughness increased with increasing laser fluence. A Sa as low as 200 nm was measured at the lowest fluence, while values up to 290 nm (best parameters) were measured for the highest fluence. In all experiments, the lowest values were associated with an optimal hatching distance of 2.575 µm (line overlap of about 63 %) and speeds that resulted in pulse overlap of 50 % or lower. Elevated values for the HD of 4.08 µm and 4.675 µm were caused by the evolved structure produced by the galvo scanner motion.

The distribution of values in the last subplot shows a clear trend in the increase of roughness with fluence. The shift of the best parameters towards higher scan speed can be explained by a) higher adequate overlap of pulses as a result of greater diameter of the material ablated and b) higher speed and number of repetitions maintain (more) uniform heat distribution and lower local temperature across the area to suppress remelting and possible chipping.

Fig. 6 summarises the results of surface roughness as a function of hatching distance for respective fluences. High error bars for the highest laser fluence were caused mainly by the very rough surface produced by the 60 mm·s·¹ speed due to remelting of ablated particles. Exact scan speed appeared to have a somewhat secondary effect on the surface texture, which could be exploited for tuning of the ablation depth after choosing a proper hatching distance.

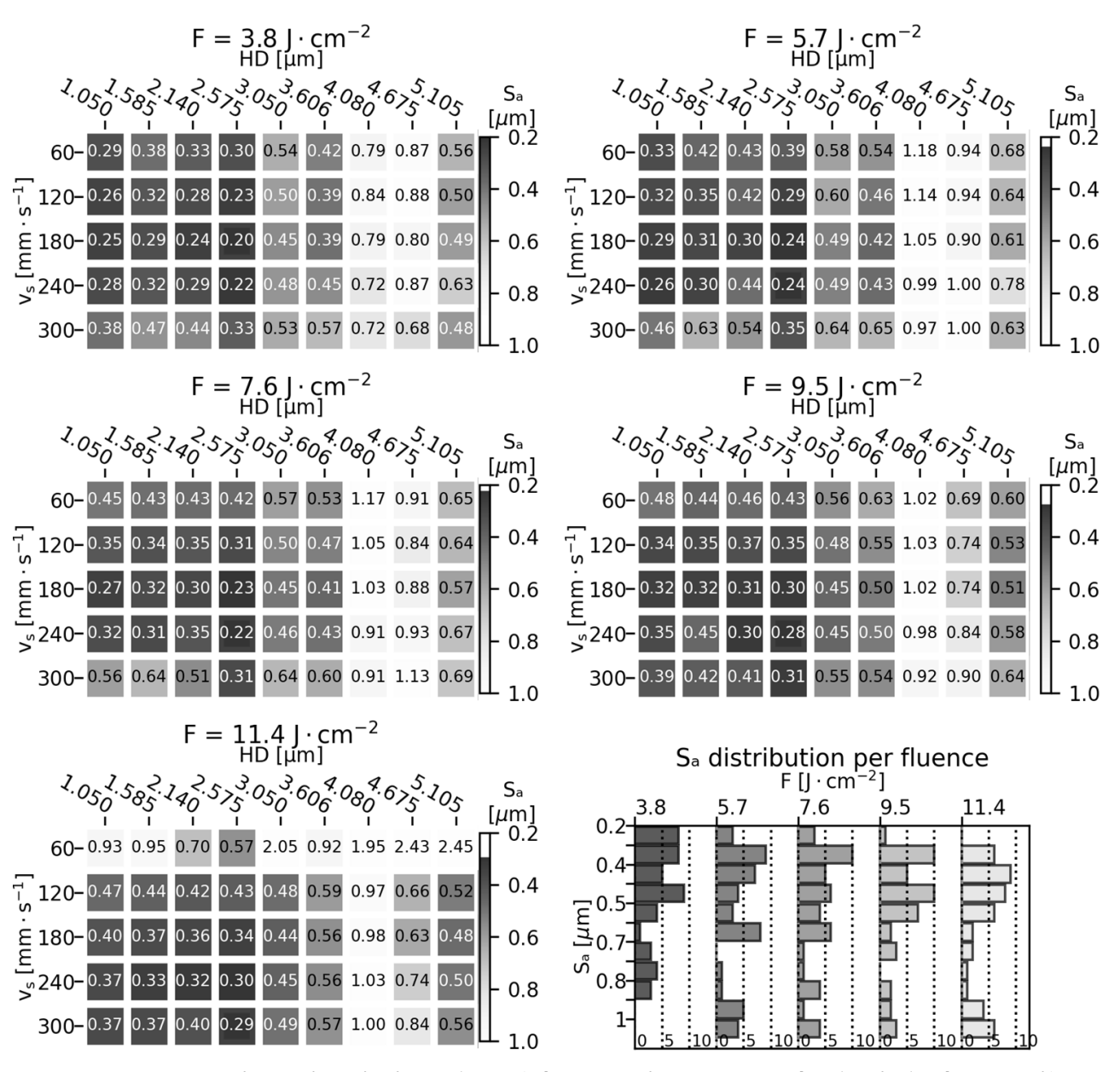


Fig. 5 Average surface roughness for the tested areas (values greater than 1 \(\mu\)m are combined in the distribution graph)

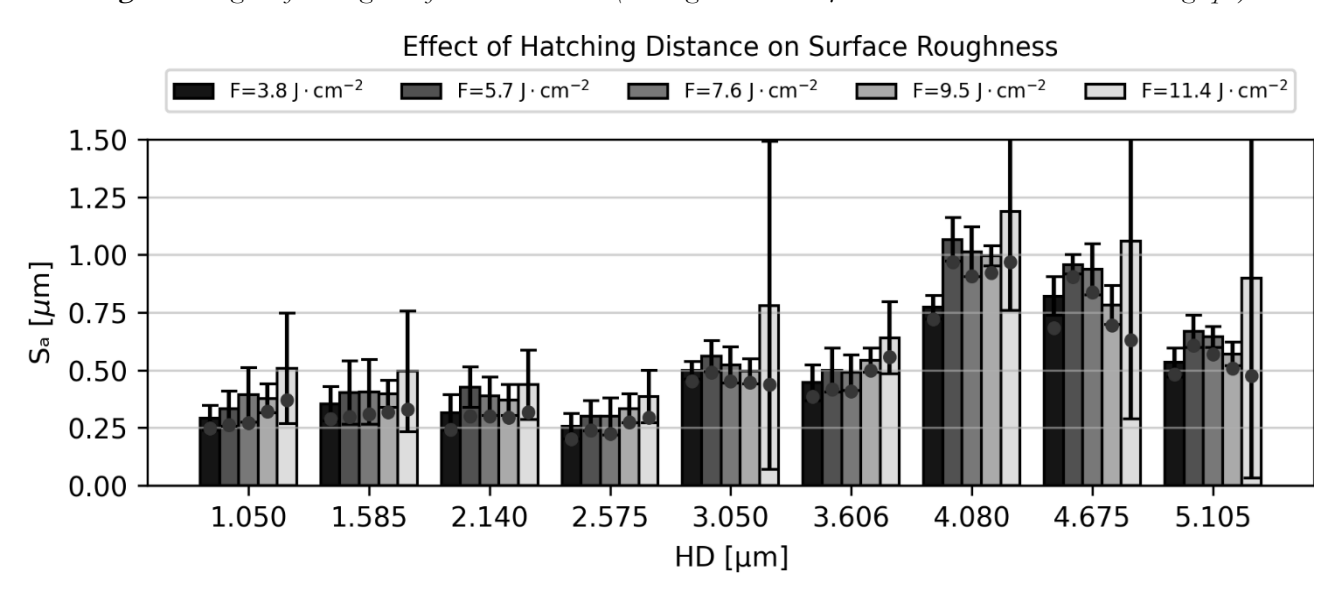


Fig. 6 Effect of hatching distance on the average of surface roughnesses (dots indicate the minimal value for respective parameters)

3.2 Material removal

The depth of the removed material was normalised to compensate for slightly different amounts of pulses among areas. Fig. 7 shows the depths for fluence of 5.7 J·cm⁻². Contrary to roughness results, the most favourable parameters did not change in response to a fluence change. The parameters for optimal roughness did not coincide with the parameters yielding the highest depth.

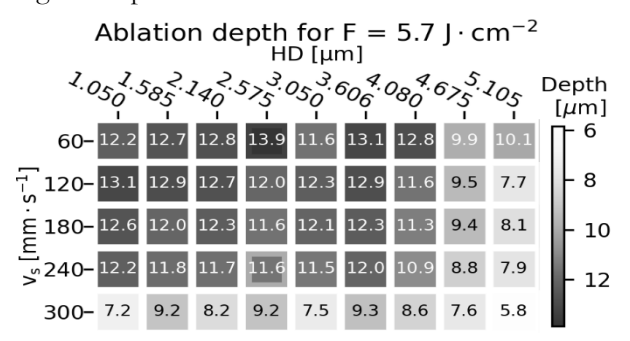


Fig. 7 Ablation depths for fluence of 5.7 J·cm⁻² (the square indicates an area with the lowest roughness)

Generally, the depth increased with increasing fluence, as illustrated in Fig. 8. The optimal speed was always found at 60 mm·s⁻¹, and it decreased with incre-

asing scan speed (decreasing overlap). This observation was caused by the accumulation effect due to a higher overlap, which resulted in a lower threshold fluence.

The most favourable hatching distance was found at $2.575~\mu m$; however, other values of HD often resulted in very similar depths without a clear trend. Fig. 9 shows the depths of ablated cavities yielding both the lowest surface roughness and highest cavity depth (and respective roughness) for individual laser fluences. Based on the graph, a slight decrease in the ablation depth could be exchanged for a rather substantial reduction in the surface roughness. To put these values into perspective, setting the lowest fluence and the roughness-optimal speed and hatching distance, it was possible to achieve layers as thin as $160~\rm nm$ per pass. The layer thickness was scalable to about $450~\rm nm$ using the laser fluence and maintaining a good roughness.

A removal rate of about 0.04 mm³·min⁻¹ (0.3 mm³·min⁻¹·W⁻¹) was achieved, which was below the reported value of about 0.45 mm³·min⁻¹·W⁻¹ achieved using an IR laser without burst mode [24]. This was probably caused by lower optical penetration depth and lower thermal effects due to lower average power, limiting chipping of larger particles from the surface.

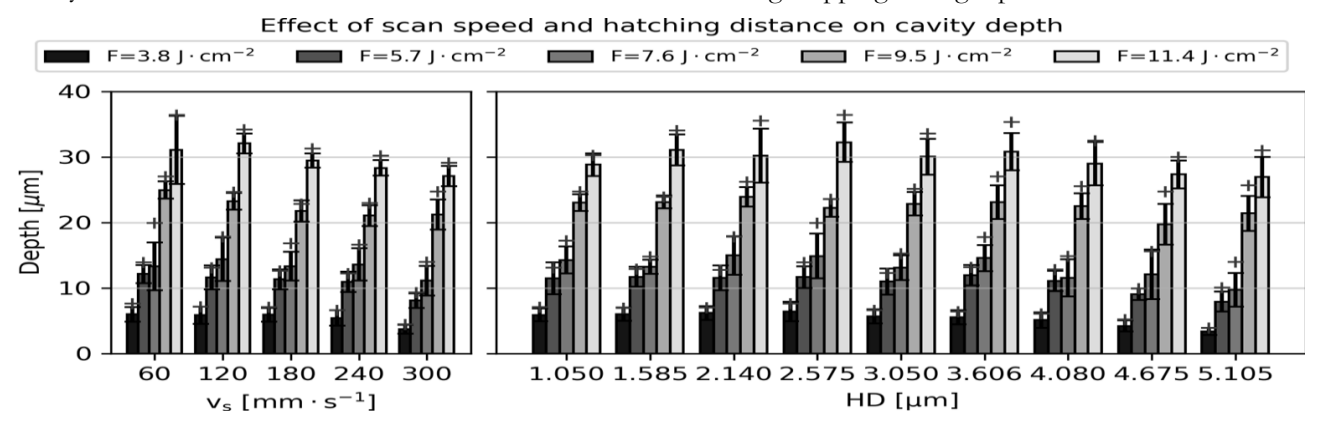


Fig. 8 Effect of speed and hatching distance on the ablation depth for different fluences (averages over the hatching distance and scan speed, respectively; points mark the highest value in the subset)

Fluence - depth - roughness relation criterion:

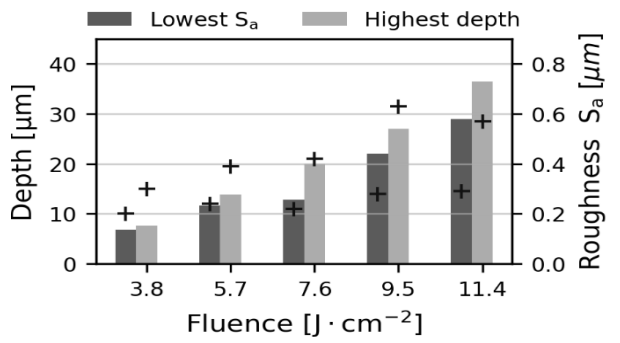


Fig. 9 Relation of the depth and roughness for areas with the lowest roughness and the highest depth for individual fluence settings

3.3 Part demonstrator

To demonstrate the applicability of the method, a sample consisting of narrow channels and slender pillars was machined. Fig. 10 shows the central section of this part. The design with outer dimensions of ca. 10 mm × 12 mm was machined to a depth of 50 µm using a fluence of 9.5 J·cm-2, a scan speed of 240 mm·s-1 and a hatching distance of 2.575 µm in a time of 60 minutes. Owing to low residual heat input and minimal defects introduced into the material, relatively high and thin pillars with a top diameter of 8 µm and a bottom diameter of 35 µm were successfully produced. Fig. 11 shows details of the area marked by a rectangle in Fig. 10 as well as the profile indicated by a line.

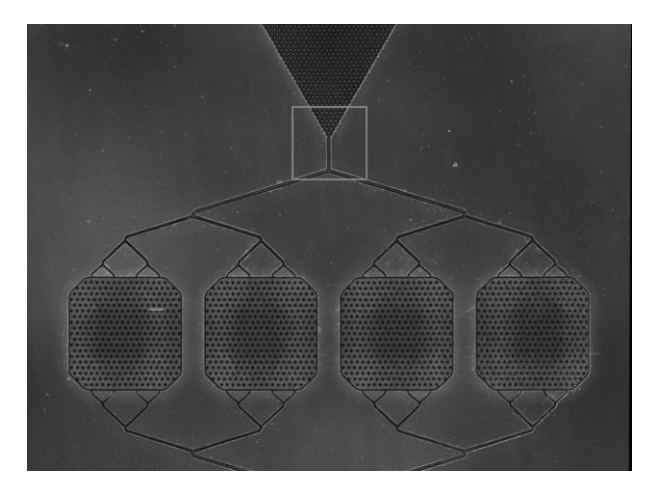


Fig. 10 Part of the manufactured demonstrator

It should be noted that this study was strongly constrained by the limited precision of the galvo scanner, which restricted the range of parameters available. Therefore, future studies should refine the process once the main issue is resolved. The second limitation was the relatively low number of fluence values and speeds tested, chosen to keep the measuring time (≈ 2 minutes per area) reasonable. Alternatives to a full factorial design, such as a fractional factorial design of the experiment or the Taguchi method, should be considered to speed up the refinement of the results [27, 28].

Although the surface quality achieved with the DUV DLW process was excellent, its productivity remains limited by the constraints of the first and second harmonic wavelengths. Nevertheless, Wlodarczyk reported that interlaced scanning of the hatching pattern improved material removal [29]. This technique could potentially double productivity, assuming all other parameters remain constant.

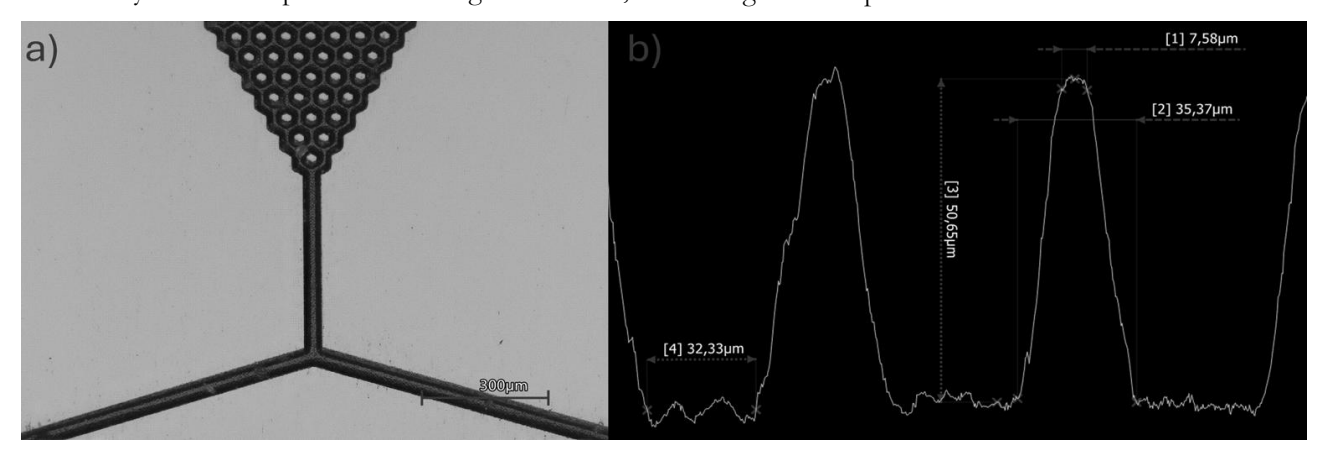


Fig. 11 Detail of the narrow channels (a) and slender pillars on the demonstrator (b)

4 Conclusion

The applicability of an ultrafast DUV laser for fused silica microprocessing was demonstrated. The process benefited from a tighter spot and better absorption, which resulted in reduced parasitic heat input into the material. This enabled machining both thin pillars and channels in the fused silica, which can be used for microfluidic devices.

A full factorial parameter study showed that surfaces with an average surface roughness of 200 nm could be produced with minimal defects in the substrate. Hatching distance was found to play an essential role in the resulting surface roughness. In this study, a line overlap of 63% provided the best roughness. To maintain good surface quality as the laser fluence was increased, a corresponding increase in the scan speed was required, from pulse overlap of nearly 60 % down to about 25 %.

Scan speed was also found to be a key parameter for the ablation depth. The deepest cavities were made using the lowest value, and the cavity depth decreased with an increase in the scan speed. This occurred due to the accumulation effect, since speed had an immediate impact on pulse overlap. A line overlap of 63 % was again beneficial for the material removal, but contrary to surface roughness, no clear trends were observed. The normalised depth of cavity, when the parameters most favourable for the surface roughness were used, ranged from 6.8 μ m to 29 μ m, depending mainly on applied fluence.

A maximum material removal rate of up to 0.04 mm³·min⁻¹ was achieved, which was lower than values typically reported for the first or second harmonic wavelength [24, 29]. This was mainly caused by a smaller focal spot size, reduced optical penetration depth and decreased chipping due to minimal residual heat input. Nevertheless, a lower material removal enabled reproducible ablation of thinner layers, which could be beneficial for a finer 2.5D slicing of various shapes.

Two distinct ablation threshold fluences were identified for polished and pre-roughened surfaces. The threshold fluence (F_{th}) of the pre-roughened surface was found to be about 35% below the F_{th} of the polished surface. This is important especially for

the processing of shallow features and machining, where the features have to be at precise depth with respect to the original surface. Optimal ablation efficiency for the pre-roughened surface was observed at about three times the threshold fluence.

A finer study of especially fluence and scan speed requires further investigation once scanner imprecision is resolved. Other strategies, such as hatching interlacing and angle variation, should be added to the scope of further studies.

Acknowledgement

This work was co-funded by the European Union and the state budget of the Czech Republic under the project LasApp CZ.02.01.01/00/22_008/0004573. The institutional support RVO:68081731 is gratefully acknowledged.

This contribution was created within the framework of project TN02000020 entitled Center of Advanced Electron and Photon Optics and is cofinanced with the state support of the Technology Agency of the Czech Republic within the Program for the Support of Applied Research, Experimental Development and Innovation of the National Center of Competence.

This research study was supported by the grant "Comprehensive technology for interdisciplinary work with advanced materials, emphasizing their multidisciplinary applications.", FSI-S-25-8787.

References

- [1] HWANG, J., CHO, Y. H., PARK, M. S., KIM, B. H. (2019). Microchannel Fabrication on Glass Materials for Microfluidic Devices. In: International Journal of Precision Engineering and Manufacturing, Vol. 20, No. 3. pp. 479–495. ISSN 2005-4602. DOI: 10.1007/s12541-019-00103-2.
- [2] CHOI, H.-K., AHSAN, Md. S., YOO, D., SOHN, I.-B., NOH, Y.-C., KIM, J.-T., JUNG, D., KIM, J.-H., KANG, H.-M. (2015). Formation of cylindrical micro-lens array on fused silica glass surface using CO2 laser assisted reshaping technique. In: *Optics & Laser Technology*, Vol. 75. pp. 63–70. ISSN 0030-3992. DOI: 10.1016/j.optlastec.2015.05.022.
- [3] LEE, P. A., LEE, U. S., SIM, D. B., KIM, B. H. (2023). Microfluidic Chip Fabrication of Fused Silica Using Microgrinding. In: *Micromachines*, Vol. 14, No. 1. pp. 96. Multidisciplinary Digital Publishing Institute. ISSN 2072-666X. DOI: 10.3390/mi14010096.

- [4] PARK, J. H., LEE, N.-E., LEE, J., PARK, J. S., PARK, H. D. (2005). Deep dry etching of borosilicate glass using SF6 and SF6/Ar inductively coupled plasmas. In: *Microelectronic Engineering*, Vol. 82, No. 2. pp. 119–128. ISSN 0167-9317. DOI: 10.1016/j.mee.2005.07.006.
- [5] KONSTANTINOVA, T. G., ANDRONIC, M. M., BAKLYKOV, D. A., STUKALOVA, V. E., EZENKOVA, D. A., ZIKIY, E. V., BASHINOVA, M. V., SOLOVEV, A. A., LOTKOV, E. S., RYZHIKOV, I. A., RODIONOV, I. A. (2023). Deep multilevel wet etching of fused silica glass microstructures in BOE solution. In: *Scientific Reports*, Vol. 13, No. 1. pp. 5228. Nature Publishing Group. ISSN 2045-2322. DOI: 10.1038/s41598-023-32503-w.
- [6] CRESPI, A., OSELLAME, R., BRAGHERI, F. (2019). Femtosecond-laser-written optofluidics in alumino-borosilicate glass. In: *Optical Materials: X*, Vol. 4. pp. 100042. ISSN 2590-1478. DOI: 10.1016/j.omx.2019.100042.
- [7] ŠILHAN, L., ARREGI, J. A., PLICHTA, T., VACULÍK, O., NOVOTNÝ, J., ŠERÝ, M. (2025). Compact vacuum setup for laser induced plasma etching with optical emission spectrum monitoring. In: *Journal of Vacuum Science & Technology B*, Vol. 43, No. 3. pp. 034202. ISSN 2166-2746, 2166-2754. DOI: 10.1116/6.0004296.
- [8] BILEK, O., ONDRIK, J., JANIK, P., KAUTSKY, T. (2024). Microtexturing for Enhanced Machining: Evaluating Tool Performance in Laser-Processed Cutting Inserts. In: *Manufacturing Technology*, Vol. 24, No. 2. pp. 173– 182. Manufacturing Technology. ISSN 12132489, 27879402.
- [9] WEBER, R., GRAF, T., BERGER, P., ONUSEIT, V., WIEDENMANN, M., FREITAG, C., FEUER, A. (2014). Heat accumulation during pulsed laser materials processing. In: *Optics Express*, Vol. 22, No. 9. pp. 11312. ISSN 1094-4087. DOI: 10.1364/OE.22.011312.
- [10] DUDUTIS, J., PIPIRAS, J., STONYS, R., DAKNYS, E., KILIKEVIČIUS, A., KASPARAITIS, A., RAČIUKAITIS, G., GEČYS, P. (2020). In-depth comparison of conventional glass cutting technologies with laser-based methods by volumetric scribing using Bessel beam and rear-side machining. In: *Optics Express*, Vol. 28, No. 21. pp. 32133–32151. Optica Publishing Group. ISSN 1094-4087. DOI: 10.1364/OE.402567.

- [11] WLODARCZYK, K., CARTER, R., JAHANBAKHSH, A., LOPES, A., MACKENZIE, M., MAIER, R., HAND, D., MAROTO-VALER, M. (2018). Rapid Laser Manufacturing of Microfluidic Devices from Glass Substrates. In: *Micromachines*, Vol. 9. pp. 409. DOI: 10.3390/mi9080409.
- [12] HUA, J.-G., REN, H., JIA, A., TIAN, Z.-N., WANG, L., JUODKAZIS, S., CHEN, Q.-D., SUN, H.-B. (2020). Convex silica microlens arrays via femtosecond laser writing. In: *Optics Letters*, Vol. 45, No. 3. pp. 636. ISSN 0146-9592, 1539-4794. DOI: 10.1364/OL.378606.
- [13] NEUENSCHWANDER, B., BUCHER, G. F., NUSSBAUM, C., JOSS, B., MURALT, M., HUNZIKER, U. W., SCHUETZ, P., (2010), Processing of metals and dielectric materials with ps-laserpulses: results, strategies, limitations and needs., DOI: 10.1117/12.846521.
- [14] TURCICOVA, H., NOVAK, O., ROSKOT, L., SMRZ, M., MUZIK, J., CHYLA, M., ENDO, A., MOCEK, T. (2019). New observations on DUV radiation at 257 nm and 206 nm produced by a picosecond diode pumped thindisk laser. In: *Optics Express*, Vol. 27, No. 17. pp. 24286–24299. Optica Publishing Group. ISSN 1094-4087. DOI: 10.1364/OE.27.024286.
- [15] ORII, Y., YOSHII, K., KOHNO, K., TANAKA, H., SHIBUYA, K., OKADA, G., MORI, Y., NISHIMAE, J., YOSHIMURA, M. (2023). High-power deep-ultraviolet light generation at 266 nm from frequency quadrupling of a picosecond pulsed 1064 nm laser with a Nd:YVO₄ amplifier pumped by a 914 nm laser diode. In: *Optics Express*, Vol. 31, No. 9. pp. 14705–14714. Optica Publishing Group. ISSN 1094-4087. DOI: 10.1364/OE.488747.
- [16] IPG PHOTONICS. (2025). IPG ULPP-2557 Deep UV Picosecond Fiber Laser. Available from: https://www.ipgphotonics.com/products/lasers/deep-uv-lasers#ftrresources
- [17] GARCIA-LECHUGA, M., UTÉZA, O., SANNER, N., GROJO, D. (2023). Wavelength-Independent Performance of Femtosecond Laser Dielectric Ablation Spanning Over Three Octaves. In: *Physical Review Applied*, Vol. 19. DOI: 10.1103/PhysRevApplied.19.044047.
- [18] FLAMM, D., SAILER, M., GROSSMANN, D., RÜBLING, S., DECKER, D., GAIDA, C., BLOTHE, M., SUTTER, D., NOLTE, S., (2025), Ultrafast laser micromachining using wavelengths from ~0.2μm to ~2μm., DOI: 10.1117/12.3042674.

- [19] HÄFNER, S., WAGNER, C., SHNIRMAN, B., GINTER, M., BRONS, J., SAILER, M., FEHRENBACHER, A., GROSSMANN, D., FLAMM, D., JANAMI, K., RUEBLING, S., QUENTIN, U., BUDNICKI, A., ZAWISCHA, I., SUTTER, D. H., (2021), Deep UV for materials processing based on the industrial TruMicro Series of ultrafast solid-state laser amplifiers., DOI: 10.1117/12.2577162.
- [20] CHO, K., CHOI, J., KO, C., KIM, M., LEE, J., EOM, E., CHO, S.-H. (2024). 257 nm Deep UV Femtosecond Laser Ablation with Minimized Crack and Chipping on Display Ultra-Thin Glass. In: *International Journal of Precision Enginee*ring and Manufacturing, Vol. 25, No. 2. pp. 271– 283. ISSN 2005-4602. DOI: 10.1007/s12541-023-00929-x.
- [21] STONYTE, D., JUKNA, V., GAILEVIČIUS, D., BALACHNINAITE, O., ZAKARAUSKAS, P., JUODKAZIS, S., (2025), Photomechanical ablation of silicate glasses using femtosecond deep-UV laser pulses., DOI: 10.1364/opticaopen.28724054.v2.
- [22] MOSKAL, D., MARTAN, J., HONNER, M. (2023). Scanning Strategies in Laser Surface Texturing: A Review. In: *Micromachines*, Vol. 14, No. 6. pp. 1241. Multidisciplinary Digital Publishing Institute. ISSN 2072-666X. DOI: 10.3390/mi14061241.
- [23] RONOH, K., NOVOTNÝ, J., MRŇA, L., KNÁPEK, A., SOBOLA, D. (2024). Effects of laser and scanning parameters on surface modification of MONEL® alloy 400 by picosecond laser. In: *Optics & Laser Technology*, Vol. 172. pp. 110514. ISSN 0030-3992. DOI: 10.1016/j.optlastec.2023.110514.
- [24] SCHWARZ, S., RUNG, S., ESEN, C., HELLMANN, R. (2021). Enhanced ablation efficiency using GHz bursts in micromachining fused silica. In: *Optics Letters*, Vol. 46, No. 2. pp. 282. ISSN 0146-9592, 1539-4794. DOI: 10.1364/OL.415959.
- [25] EN ISO 25178-3, (2012), Geometrical product specifications (GPS) -- Surface texture: Areal -- Part 3: Specification operators.
- [26] REDKA, D., VELA, S., SPELLAUGE, M., MINÁR, J., MORALES, M., MOLPECERES, C., HUBER, H. P. (2025). Improved prediction of ultrashort pulse laser ablation efficiency. In: *Optics & Laser Technology*, Vol. 189. pp. 113103. ISSN 0030-3992. DOI: 10.1016/j.optlastec.2025.113103.

- [27] JABBAR, M. A. (2023). A Design of Experiment Analysis Approach to Improve Part Quality in 3D Printing. In: *Manufacturing Technology*, Vol. 23, No. 3. pp. 290–297. ISSN 12132489, 27879402. DOI: 10.21062/mft.2023.034.
- [28] SIREGAR, I., SAEDON, J., SHAHRIMAN ADENAN, M. (2025). Milling Performance of Selective Laser Melted Ti6Al4V: A Taguchi Approach for Surface Roughness Optimization. In: *Manufacturing Technology*, Vol. 25, No. 2. pp. 230–238. ISSN 12132489, 27879402. DOI: 10.21062/mft.2025.030.
- [29] WLODARCZYK, K. L., LOPES, A. A., BLAIR, P., MAROTO-VALER, M. M., HAND, D. P. (2019). Interlaced Laser Beam Scanning: A Method Enabling an Increase in the Throughput of Ultrafast Laser Machining of Borosilicate Glass. In: *Journal of Manufacturing and Materials Processing*, Vol. 3, No. 1. pp. 14. Multidisciplinary Digital Publishing Institute. ISSN 2504-4494. DOI: 10.3390/jmmp3010014.